NASA Technical Memorandum 101306

# Application of Optical Correlation Techniques to Particle Imaging Velocimetry

Mark P. Wernet
*Lewis Research Center*
*Cleveland, Ohio*

and

Robert V. Edwards
*Case Western Reserve University*
*Cleveland, Ohio*

**NASA**

# Application of Optical Correlation Techniques to Particle Imaging Velocimetry

Mark P. Wernet

NATIONAL AERONAUTICS AND SPACE ADMINISTRATION

Lewis Research Center

Cleveland, Ohio 44135


Robert V. Edwards

Case Western Reserve University

Cleveland, Ohio 44106

## Abstract

Pulsed laser sheet velocimetry yields non–intrusive measurements of velocity vectors across an extended 2–dimensional region of the flow field. The application of optical correlation techniques to the analysis of multiple exposure laser light sheet photographs can reduce and/or simplify the data reduction time and hardware. Here, Matched Spatial Filters (MSF) are used in a pattern recognition system. Usually MSFs are used to recognize characters or assembly line parts. In our application, the MSFs are used to identify the iso–velocity vector contours in the flow. The patterns to be recognized are the recorded particle images in a pulsed laser light sheet photograph. Measurement of the direction of the particle image displacements between exposures yields the velocity vector. In this work, the particle image exposure sequence is designed such that the velocity vector direction is determined unambiguously. A global analysis technique is used in comparison to the more common particle tracking algorithms and Young's fringe analysis techniques.

## Introduction

The technique of recording multiple speckle pattern translations that occur during surface motion has become a useful tool to measure in–plane displacements of solid surfaces.[1,2] Current interests are focused on applying this technique to the measurement of particle displacements in 2–D fluid flow fields.[3-8] Double pulsing a laser light sheet perpendicular to the direction of observation yields a record of the particle positions at two instances of time over the entire plane. The number density and size of particles in the fluid determines the data analysis approach. For a large number density of recorded particle images, the laser speckle data analysis procedure is used. This technique is called Laser Speckle Velocimetry (LSV). In LSV, the recorded particle photographs are usually analyzed by illuminating small regions by a low power laser beam. The far field diffraction pattern of the illumination beam contains speckly Young's fringes. The fringes are oriented perpendicular to the local velocity vector, and the fringe spacing is inversely proportional to the velocity magnitude. Measurement of the fringe spacing and orientation gives the local velocity vector. By repeating the process over a grid of points on the transparency, a 2–D velocity vector map is constructed. For low number density double pulsed photographs, different processing schemes are applied. These low number density processing techniques are referred to as Particle Imaging Velocimetry (PIV). Due to the low particle density, individual particle displacement vectors can be determined, instead of the average displacement of a group of particles as in laser speckle. Particle tracking algorithms employing image processing techniques can be used to reduce the recorded PIV transparencies. Alternatively, the point–wise laser beam readout technique can be used to determine the local velocity vectors. Hence, different processing schemes may be applied depending on the recorded particle number density.

The point–wise laser beam readout of a recorded particle image transparency is a tedious and time consuming process. The point–wise analysis of the transparency is similar to laser anemometry techniques. In their present state, both PIV and LSV techniques are similar in nature to the point–wise measurements obtained using laser anemometry, which are time consuming and have positioning constraints.

For a typical 100cm² region of a transparency analyzed on a 1mm grid, there are on the order of $10^4$ points to be analyzed. At each point, the far field fringe pattern spacing and orientation must be determined. This exhausting data analysis technique is most efficiently handled by an automated procedure. However, even an automated procedure employing specialized array processors can still require hundreds of hours of processing time.

For all of the effort that has been expended to analyze the particle image transparencies and determine the fringe spacing and orientation at $\approx 10^4$ points, there still exists a 180° directional ambiguity. The fringe patterns generated by the readout beam are symmetric, hence, the velocity vector is known only to ±180°. More information must be included at the recording stage of the process to resolve the direction unambiguously.

In this paper, we describe a 2–D optical parallel processing technique for analyzing recorded PIV transparencies with unambiguous velocity vector determination. The techniques of Matched Spatial Filtering used in character recognition systems are employed to identify individual particle image records. The directional ambiguity dilemma is eliminated by using an asymmetric laser light sheet exposure sequence.

The optimal exposure pattern must yet be determined. Three unevenly spaced pulses yield enough information for determining the flow direction, but also can result in many false correlations. Other less ambiguous patterns are being investigated. The analysis procedure can be done optically using a magnetooptical spatial light modulator. The light modulator is used to display Hartley Binary Phase Only Filters (HBPOF) used in an optical correlator. The BPOFs are written on the light valve through a computer interface. Light valves with 128×128 elements are currently available. Alternatively, the photographs to be analyzed can be digitized and the MSF process performed digitally using Fast Fourier Transforms. This approach requires supercomputing facilities, or specialized array processors, but does not suffer from the limited spatial resolution of the commercially available light valves.

## PIV and LSV

Double pulsed velocimetry enables the instantaneous recording of the in–plane velocity vectors across an entire 2–D flow field, see figure 1. The fluid under study is seeded with small particles. Illumination is supplied by a thin sheet of double pulsed laser light. The particle positions at these two instances of time are recorded on a photographic plate. A switched or pulsed laser source supplies the light pulses. The pulse lengths, $\delta t$, are usually on the order of 20–30 nanoseconds.[8] The short pulses are needed to record the images of the micron sized particles before they move enough to distort the image. The pulsing interval $\Delta t$, which can range from $\mu s$ to seconds, is chosen based on two criteria: 1) to limit the maximum particle in–plane displacements to a desired value, and 2) to limit the out–of–plane displacement to less than the light sheet thickness $\Delta z$. The first criterion ensures that the recorded images are not so far apart on the image plane that a practical data analysis procedure cannot be used. The second restriction merely insures that most of the particles are within the illumination volume during both pulses.

There are major differences between the application of laser speckle to surface displacements and particle displacements. The main difference is that the light scattering properties of small particles suspended in a fluid are distinctly different than the light scattering characteristics of a solid surface. The fluids are illuminated by a light sheet of finite thickness $\Delta z$. Hence scattering occurs from a volume distribution of scattering sites instead of a surface distribution. The scattering particles are usually small ($0.1\mu m$ to $10\mu m$). The number density and particle size vary depending on the fluid and the application.[9]

For speckle patterns to occur, the number of scattering sites per unit volume must be high enough so that the diffraction limited images overlap in the image plane.[5,8] If the number density of particles is low, or if the scattering properties of the particles are insufficient for exposing the photograph, laser speckle may not be

obtained, but discrete particle images may be recorded instead. In either case, one must choose the best technique for reducing the data. Although there are some techniques which attempt particle tracking, most approaches rely on the beam readout technique. The beam readout technique can be used for both the PIV and LSV recording regimes. The photographic transparency is divided up into a grid of points. A typical photograph may contain $10^4$ grid points. At each grid point a low power laser beam is used to illuminate a small region, ($\approx 1mm$ diameter). The particle images within the illuminated region act as paired sources producing Young's fringes in the far field. The fringe pattern spacing is inversely proportional to the average particle displacement within the illumination region. The orientation of the fringes is perpendicular to displacement direction. The Young's fringe patterns are digitized by a CCD camera and processed in a computer. The processing techniques vary depending on the available hardware, but the primary operation is to Fourier transform the fringe pattern. The Fourier transformed fringe pattern is used to compute the power spectral density of the fringe pattern. The power spectral density is a symmetric function containing three peaks, see figure 2. The displacement of the side peaks from the origin peak is proportional to the velocity. The beam readout technique does not directly provide any information on the sign of the velocity vector direction. The estimated vector at each interrogation region is known only to $\pm 180°$.

A similar approach is to compute a select number of 1–D autocorrelations instead of the 2–D autocorrelation. This significantly reduces the number of computations. The 1–D autocorrelations are obtained by integrating the 2–D interrogation regions along the x– and y–axes. The integration can be done either numerically in the computer after digitization by a 2–D CCD array, or optically using cylindrical lenses before digitization by two 1–D CCD arrays.[10] The particular approach will depend on available hardware, although the optical integration will be faster. After the 1–D projections of the 2–D interrogation region are obtained, 1–D autocorrelations are computed to determine the x– and y–components of the local velocity vector. These 1–D analysis techniques work well when only a single particle image pair is present in the interrogation region. When more than two images are present, some spurious peaks can arise in the autocorrelations, which can lead to indeterminate velocity vectors.

A basic problem with all of these PIV and LSV data reduction techniques is the directional ambiguity. The particle tracking algorithms can determine the velocity magnitude, but a $\pm 180°$ angle ambiguity still remains. Two modified PIV techniques which address the directional ambiguity problem are the image shifting technique[11,12], and holographic image separation.[13]

In the image shifting technique, the image field is shifted between the two illumination pulses, such that the second image of every particle image pair is rectilinearly displaced from the first image. A mirror mounted on a galvanometer scanner in the recording system optical path enables the image shift between pulses. The magnitude and direction of the image shift is set such that even the most negative velocities are still positively displaced. This image shifting aids in the particle tracking algorithms since it sets a bound on the most probable position for the second particle image. For example, if the shift is a positive upward shift to the right, the tracking program knows to look for the second

particle image up and to the right of the first image. The sign of the velocity is assigned based on the magnitude of the measured displacement. Displacements larger than the rectilinear image shift are positive velocities, while displacements smaller than the shifted distance are negative.

The holographic image separation technique permits the unambiguous identification of the first and second particle images. The double pulsed particle images are recorded holographically on a photographic plate. Two separate reference beam arrangements are used for each exposure. In this way, the first and second positions of all the particles can be viewed separately by subsequent reconstruction using the two reference beams. The separation of the particle images permits the computation of the cross correlation function which gives the displacement and unambiguous direction information.

All of these techniques discussed are either computationally intensive or have limited applicability, and yet very few offer unambiguous direction determination. There is a strong need for a fast data reduction technique which also provides unambiguous direction information.

Matched Spatial Filtering

Pattern recognition is a widely investigated optical processing technique. The purpose of a pattern recognition system is to determine the presence and location of a reference pattern in an input scene. The primary operation in a pattern recognition system is the correlation of an input scene with a reference pattern. A matched spatial filter is the optimum filter for pattern recognition since it maximizes the ratio of the peak signal energy to the mean square noise energy in the output of the processing system. The signal is any object of interest in the scene, and the noise is the rest of the image.

A coherent optical processing system, shown in figure 3, is capable of performing optical pattern recognition. The correlation is performed by multiplying the Fourier transforms of the input scene and a reference pattern, followed by an inverse Fourier transform. Lenses are used to perform the optical Fourier transforms. In a coherent optical processor, the complex conjugate of the Fourier transformed reference pattern is stored on a transparency. Since the transparency containing the reference pattern is placed in the Fourier plane, it is a spatial filter. The stored reference pattern is a complex electric field and is similar to a hologram. In this text, a spatial filter will be any transparency or waveform modulating device placed in the filter plane of an optical correlator, or simulated optical correlator system.

When the transparency containing the input scene is placed at the input plane of the coherent optical correlator, the output plane contains the light intensity distribution from the convolution of the reference pattern with the input scene. If the input scene transparency contains the reference pattern, the output of the system essentially represents the probability that the desired signal has occurred in the input scene. A bright spot in the output plane indicates a high probability of occurrence at that position, a dim spot indicates a low probability. This process simultaneously detects signals with similar orientations regardless of their position in the input scene. This space invariance results from the

fact that the spectrum of a translated signal is only modified by a linear phase factor. The phase factor contains the necessary information to image the signal probability of occurrence at the proper position in the output plane. However, the system is sensitive to the relative orientation of the input signal with respect to the filter. The input scene can be scanned for all possible orientations of the signal by rotating the filter to all possible orientations.

More formally, the input scene transparency placed at plane $P_1$ is Fourier transformed by lens $L_2$. Let the input scene transparency contain the signal function $s(x,y)$. The Fourier transform of the input scene transparency $S(p,q)$ is defined as:

$$S(p,q) = \iint_{-\infty}^{\infty} s(x,y) \cdot e^{-i(px+qy)} \, dx \, dy \qquad (1)$$

The electric field, $S(p,q)$, is imaged onto a transparency containing a matched spatial filter at plane $P_2$, which is also called the filter or Fourier plane. The MSF contains $F^*(p,q)$ and (unavoidably) some other terms. Propagating an electric field through a transparency is equivalent to multiplying the complex transmittance function contained in the transparency, $F^*(p,q)$, by the electric field passing through the transparency. The multiplication operation performs the spatial filtering. The filtered signal $S(p,q) \cdot F^*(p,q)$ is then inverse Fourier transformed by lens $L_3$. The resultant electric field is observed at the output plane $P_3$, and is given by:

$$\mathcal{E}_0(x,y) = \frac{1}{4\pi^2} \iint_{-\infty}^{\infty} S(p,q) \cdot F^*(p,q) \cdot e^{i(px+qy)} \, dp \, dq$$
$$(2)$$

When $S(p,q)$ is located in the input scene and the MSF contains $F^*(p,q) = S^*(p,q)$, we see that the electric field at plane $P_2$ is pure real, since the conjugate phases cancel. The cancellation of the phase gives a uniform illumination at plane $P_2$ (a planar wavefront), which when Fourier transformed by $L_3$, gives a delta function response. This bright spot occurs on the output plane corresponding to the location of $s(x,y)$ in the input transparency.

The MSF that we have assumed here is a simplified version of the actual case. In reality, the complex waveform $F^*(p,q)$ can only be recorded on a transparency by using a high frequency carrier. The high frequency carrier is easily obtained using a planar off-axis reference beam.[14] Using a reference beam to record the complex waveform increases the space-bandwidth requirements on the photographic recording transparency. The interferometrically recorded MSF actually contains:

$$F_{MSF}(p,q) = |R(p,q)|^2 + |F(p,q)|^2 + R^*(p,q)F(p,q)$$
$$+ R(p,q)F^*(p,q) \qquad (3)$$

where $R(p,q)$ represents the an off-axis reference electric field, and $F(p,q)$ represents the filter pattern spectrum. The equation above contains three separable terms. The first two terms together make up a dc spot. The third term contains the filter spectrum multiplied by a linear

phase factor. The fourth term, which is the term of interest, represents the complex conjugate of the filter spectrum multiplied by the another linear phase factor. The output electric field obtained on plane $P_3$ is:

$$\mathcal{E}_o(x,y) = \frac{1}{4\pi^2} \int\limits_{-\infty}^{\infty}\int F_{MSF}(p,q) \cdot S(p,q) \cdot e^{i(px + qy)} dp\, dq$$

(4)

which yields at the output plane of the optical correlator:

$$\mathcal{E}_o(x,y) = r_o^2 \cdot s * \delta(x,y) + [f*f*s] * \delta(x,y)$$
$$+ r_o \cdot [s*f*\delta(x-b, y-c)]$$
$$+ r_o \cdot [s*f*\delta(x+b, y+c)] \quad (5)$$

where b and c are constants determining the reference beam incidence angle. In equation 5, the first term, which contains two parts, represents a dc spot that occurs on–axis (x=0,y=0) in the output plane. The Fourier transform of the collimated reference beam $R(p,q)$ is a point $r_o$. The second term represents the convolution of the filter function with the input scene (s*f). This term appears off–axis at position (x=b,y=c). The third term, which is the one of interest, is exactly the expected output from the optimum filter. This term represents the cross correlation of the input scene with the filter function (s*f) and appears on the output plane at (x=–b,y=–c). When s=f a maxima occurs on the output plane.

### Phase Only And Binary Phase Only Filters

Since Vander Lugt's original introduction of MSFs there has been considerable effort devoted to the study of optical correlators. Analysis of the Fourier transform of continuous tone pictures has revealed that the phase information is considerably more important than the amplitude information.[15] Classical Vander Lugt MSFs use both amplitude and phase information. The amplitude portion of the MSF alters the amplitude transmission of the spatial filter. This amplitude modulation decreases the light transmitting efficiency of the MSF. A purely Phase Only Filter (POF) has 100% transmission efficiency. The incident light is not attenuated, but the phase is modulated across the plane. Hence, POFs may offer an alternative to classical MSFs for optical correlator systems requiring high transmission efficiency.

Successful results using POFs in optical correlator experiments have been reported.[16,17,18] The performance of a POF can be described mathematically by using a combination of a classical MSF and an amplitude transmittance filter. Let the MSF response function be written in polar form:

$$F(p,q) = |F(p,q)| \cdot e^{i\phi(p,q)} \quad (6)$$

where $|F(p,q)|$ is the magnitude of $F(p,q)$, and $\phi(p,q)$ is the phase of $F(p,q)$. A POF can be obtained by inserting an amplitude transmittance filter containing the inverse amplitude of the MSF $(1/|F(p,q)|)$ in front of the MSF. When these two filters are placed in series, the two amplitudes cancel, producing unity amplitude transmittance. The phase only response is then:

$$F_{POF}(p,q) = e^{i\phi(p,q)} \quad (7)$$

A spatial filter obtained by combining a MSF and an amplitude transmittance filter in this manner will aid in revealing the properties of the POF. The Fourier spectra of finite, real valued objects fall off with increasing frequency. The amplitude only filter preceding the MSF will have a reciprocal response behaving similar to a high pass filter. High pass filtering is a standard image processing technique to emphasize edge information. The correlation peaks obtained using POFs in optical correlators are very sharp, since the high spatial frequency information decorrelates very quickly. This high frequency emphasis also makes the POF more sensitive to scale and rotation changes than a conventional MSF. Although the POF can produce sharper correlation peaks with lower sidelobes, the MSF is still the optimum filter in the presence of noise.

Phase only filters can be generated by bleaching a previously developed photographic plate, or by using a plate with a dichromated gelatin emulsion. However, restricting the continuous phase filter function to binary values offers several advantages. A binary process is easy to control and the two phase levels can be set very accurately. Another advantage of using a binary phase only filter is the elimination of the dc spot in the output of an optical correlator system. These binary filters can be digitally generated on a computer, which eliminates the complex optical preprocessing required in MSF synthesis, or in the synthesis of continuous POFs.

Binary Phase Only Filters (BPOF) are generated in a two step process. First the discrete Fourier transform $F(p,q)$ of the function to be searched for, $f(x,y)$, is calculated. Then the BPOF, which will be referred to as $F_{BPOF}(p,q)$ is made by setting the phase at each point $(p,q)$ to one of two levels, depending on the sign of the cosine of the phase angle in $F(p,q)$. A technique proposed by Psaltis[18] for generating BPOFs is:

$$F_{BPOF}(p,q) = \begin{cases} +1 & \text{if } Re[F(p,q)] > 0 \\ -1 & \text{otherwise} \end{cases}$$

The Psaltis technique is equivalent to taking the cosine transform $F_C(p,q)$ of $f(x,y)$ and then determining $F_{BPOF}(p,q)$ by:

$$F_{BPOF}(p,q) = \begin{cases} +1 & \text{if } F_C(p,q) > 0 \\ -1 & \text{otherwise} \end{cases}$$

The performance of the BPOF in an optical correlator can be demonstrated by considering the continuous cosine transform of $f(x,y)$. The cosine transform can be written:

$$F_C(p,q) = \frac{1}{2}[F(p,q) + F^*(p,q)] \quad (8)$$

where for real $f(x,y)$:

$$F(p,q) = \mathscr{F}\{f(-x, -y)\}^* \quad (9)$$

where $\mathscr{F}\{\}$ denotes the Fourier transform operation and * denotes complex conjugation. Equation 8 shows that whenever $F_C(p,q)$ is used in an optical correlator, the input scene will be correlated with both $f(x,y)$ and $f(-x,-y)$.

The optically recorded MSF had to be recorded using a spatial carrier in order to get the terms of interest off-axis, away from the dc spot. Since no spatial carrier is required for separating the outputs, the space-bandwidth product of the recording medium is substantially reduced. So we see that the BPOF yields two terms off axis, without the use of a spatial carrier, and without any optical processing.

The BPOFs discussed above do not always perform well for cases where the input scene contains large amounts of clutter or objects. The BPOFs can cause the objects to interfere with each other, which causes a variation in the correlation peak amplitudes on the output plane. An alternative to the BPOF is the Hartley-BPOF, or HBPOF. The HBPOF is constructed in a similar two step process as the BPOF, except that the Hartley transform is used instead of the Fourier transform. The Hartley transform can be defined for real valued input functions as:[20]

$$H(p,q) = Re\{F(p,q)\} - Im\{F(p,q)\} \qquad (10)$$

where $F(p,q)$ is the Fourier transform of the real valued filter function $f(x,y)$. The HBPOF is generated by:

$$F_{HBPOF}(p,q) = \begin{cases} +1 & \text{if } H(p,q) \geq 0 \\ -1 & \text{otherwise} \end{cases}$$

The HBPOFs seems to perform very much the same as the BPOFs, with the exception of having much lower variation in correlation peak amplitude.[20]

## Spatial Light Modulators

A coherent optical correlator requires a spatial filter for proper operation. A matched spatial filter is the most common type of filter used in an optical correlator. Making the MSFs requires much care, preparation, and trial and error. Yet each MSF is capable of only recognizing a single object pattern. Processing the input scene using optically recorded MSFs requires many transparencies. The BPOFs can be synthesized entirely on a digital computer. The exact object function is not required to be Fourier transformable since the discrete Fourier transform contains sufficient information for generating the BPOFs. The cosine of the phase of the original Fourier transformed function is analyzed at each point, and assigned one of two discrete phase values. The BPOFs are more sensitive to scale and rotation changes than conventional continuous, complex valued MSFs.[16] These properties alone do not make the use of BPOFs in coherent optical processors attractive. However, with the advent of high speed two-dimensional spatial light modulators, BPOFs can be readily synthesized in the computer and encoded onto the light modulator for use in coherent optical correlator systems.

There are several types of spatial light modulators available. Some of these are optically addressable and use liquid crystal light valves.[21-23] Other electronically addressable liquid crystal displays are used in small portable televisions.[24-26] Semetex corporation manufactures a SIGHT-MOD magnetooptic spatial light modulator.[27] The SIGHT-MOD uses the Faraday effect to selectively rotate the polarization of the transmitted linearly polarized coherent light. The SIGHT-MOD consists of a matrix of small elements, or pixels. Each pixel can operate independently, so that the light incident over the two-dimensional area of the SIGHT-MOD can be locally modulated. Depending on the orientation of the output polarizer, both binary amplitude modulation, or binary phase modulation can be obtained. The binary phase modulation operational mode permits the construction of BPOFs on the SIGHT-MOD. The SIGHT-MOD is electrically addressable through a computer interface. The device is capable of displaying several frames per second. The largest matrix size available is a 128×128 element device. As pointed out before, BPOFs do not require high space-bandwidth products in order to obtain good performance.

Through the development of these high speed, electrically addressable, binary phase modulators, coherent optical correlator systems can be constructed which employ BPOFs at the filter plane.[19,20,28-40] Such a coherent optical correlator system is capable of generating the interrogation patterns inside the computer, and then displaying the BPOFs on the spatial light modulator. The input scene is interrogated by displaying successive filter response functions on the light modulator. Hence, the true potential of pattern recognition systems sensitive to object shape and rotation can be obtained using 2-D spatial light modulators employing BPOFs for signal detection.

## Optical Correlations For Particle Imaging Velocimetry

Optical correlator systems have been employed to identify a wide class of objects including: alpha numeric characters, assembly line parts, human faces, military aircraft, ships, tanks, and multiple exposure particle image records.[16,18-20,41,42] In our application, an optical correlator will be used to identify recorded particle images from a multiple-pulse laser light sheet technique. The pulsed laser sheet technique, also called Particle Imaging Velocimetry (PIV), records the in-plane particle positions at the instants the light sheet is pulsed. Typically, two pulsed light sheets are used, yielding two records of each particle in the light sheet. The individual particle displacements between exposures is proportional to the in-plane velocity component of the particle. This two pulse recording scheme results in a 180° directional ambiguity when traditional point-wise Young's fringe analysis or autocorrelation techniques are used to reduce the data. When the photographic transparency containing the recorded particle images is placed at the input plane of a coherent optical correlator system, the entire photograph can be processed in parallel. In addition to speeding up the data reduction process, the optical correlator can be used to determine the velocity vector directions unambiguously. The directional ambiguity is removed by using the appropriate pulsing scheme.

A pulsing sequence yielding a non-symmetric pattern can be used to eliminate the directional ambiguity. The problem is to determine the optimum pulsing sequence which gives good signal discrimination on the output plane, unambiguous velocity direction information, and a low number of false correlations. A triple pulse light sheet scheme can be used with non-symmetric time periods between the pulses. The asymmetry enables the particle direction to be unambiguously determined. For example, let $\Delta t_{12} = 2 \cdot \Delta t_{23}$ where $\Delta t_{12}$ is the time interval between pulses 1 and 2, and $\Delta t_{23}$ is the time interval between pulses 2 and 3. The corresponding recorded

particle image sequence for a left to right flow direction is:

• • •

This exposure sequence yields unambiguous direction information. However, this is not the traditional exposure technique used in PIV and LSV approaches. Typically, the time intervals are equally spaced. The asymmetric spacing in the recorded particle image triplet above produces a fringe pattern with 3 frequency components. The phase information from the 3—pulse pattern contains the direction information. The traditional PIV and LSV data reduction techniques use the squared modulus of the fringe pattern to obtain the velocity information. The squared modulus of the fringe pattern retains no phase information. Hence, the conventional PIV and LSV techniques are unable to make use of the 3—pulse encoded phase information for directional ambiguity removal. A coherent optical processor is able to use the phase information from the 3—pulse pattern to determine the velocity direction unambiguously.

Another recording scheme could consist of a 5—pulse pattern. The ratio of the spacings is 2:2:1:1. The recorded pattern is shown below for a left to right flow:

• • • • •

The 5—pulse pattern can be generated by shuttering a continuous pulsed laser source.

The 3— and 5—pulse exposure sequence particle image photographs can be reduced using an optical correlator. Individual particle displacement records for each particular velocity magnitude and flow direction are used to make the spatial filters in the PIV optical correlator. Spatial filters are made to cover the expected range of velocity magnitude and flow direction.

Using conventional MSF techniques would require making individual MSFs for each expected velocity vector on the input scene. This could easily escalate into an unmanageable number of MSFs to store and manipulate. Sequentially positioning large numbers of MSFs into the frequency plane of the optical correlator would be extremely tedious and time consuming.

Alternatively, an electronically addressable spatial light modulator can be used to display MSFs in the frequency plane of an optical correlator. The relatively low spatial frequency content of the Fourier spectra of the 3— and 5—pulse exposure sequences are well suited for the BPOF technique. The BPOFs can be used instead of MSFs since we do not have a detailed signal nested in a complex background. Our noise is the random location of independent particle image records on the input scene transparency. The BPOFs can be synthesized in the computer without any optical processing, and are readily encoded onto a magnetooptic spatial light modulator through a computer interface. A spatial light modulator placed in the frequency plane of the PIV optical correlator can sequentially display the BPOFs which have been previously generated and stored in the computer. A CCD array camera placed at the output plane in the optical correlator digitizes the light intensity distribution for analysis in the computer.

Computer Simulation of Optical Correlators

The optical correlation system discussed for analyzing PIV photographs can easily be simulated on a digital computer, although the simulation is computationally intensive. Two simulation programs were written. One computer simulation was written on a high performance personal computer (pc) to analyze the output plane light intensity distribution of the optical correlator. The second simulation program was written to simulate the sequential scanning of the input scene for successive velocity vectors. This second simulation program was executed on a CRAY—XMP supercomputer. The 2—D velocity vector maps were obtained from the CRAY simulations.

The programs can be easily modified to select different types of spatial filters (MSF, POF, BPOF, and HBPOF) and/or different types of interrogation patterns (3—pulse or 5—pulse). The MSFs used in the computer simulations are defined as the complex conjugate of the filter pattern spectra. The ease in modifying the program permits the analysis of different filtering techniques without the trial and error process of optically recording the filters. The optical Fourier transforms performed by lenses in the optical correlator are obtained in the simulation by using Discrete Fourier Transforms (DFT). The DFT closely approximates the actual Fourier transform. The Fast Fourier Transform (FFT) is a computationally efficient DFT and was used in the computer simulations. The pc simulation program will be discussed first to gain an understanding of the expected output light intensity distribution from the optical correlator. Then the CRAY simulations will be discussed along with the program output 2—D velocity field map.

The pc simulation of the optical correlator system uses a 64×64 element input scene, zero padded[43] to 128×128 elements. The zero padding eliminates the wraparound error, but also increases the CPU time. A flow sheet for the simulation is given in figure 4a. The program queries the user for the number of particle image recordings in the input scene. The data are entered in the same format regardless of whether the recording scheme is the 3— or 5—pulse. The data for each particle image recording on the input transparency are entered as: the $(x,y)$ coordinates of the mean position of the recorded image on the input scene; S1—the spacing between images 1 and 2 (or the spacing between exposures 1, 2, and 3 for the 5—pulse case); S2—the spacing between images 2 and 3(or the spacing between exposures 3, 4, and 5 for the 5—pulse case); and the angular orientation of the particle image record, $\theta$. For the triple pulse case, the program determines the coordinates of each particle image and places a value of unity at each location in the input scene array, see figure 5. The total power from each particle image triplet is 3.0. For the 5—pulse case, the program again places a value of unity at each particle image position, see figure 6. The energy content for the 5—pulse pattern is 5.0. After all of the input scene data have been entered, the 2—D FFT of the input scene is computed. Next, the spatial filter pattern is computed. The parameters describing the spatial filter are stored as constants within the program. The coordinates of the particle image positions in the filter pattern array are computed, a value of unity is placed at each position within the array, and the filter pattern is Fourier transformed. The complex conjugate of the Fourier transformed filter pattern is the MSF, and can be stored in a complex array in the simulation. Recall that the optical recording of an MSF required an off—axis reference beam to record the complex waveform. The MSFs are generated and stored very easily in the computer simulation.

At this point in the program, the spatial filter can be modified to some type other than the classical MSF. When optically recording a MSF for use in an actual

6

optical correlator, one tries to maximize the transmittance of the MSF. The higher the transmittance, the more optically efficient the MSF. The MSF optical transmittance calculated in the computer simulation is maximized by normalizing the computed MSF such that the maximum transmittance is unity. The MSF is scanned and the maximum transmittance value, $F_{max}$, is determined. All points in the MSF are divided by the maximum amplitude transmittance of the filter, $F_{MSF}(p,q) = F^*(p,q)/F_{max}$. The resulting continuous valued MSF contains transmittance values from 0 to 1. MSFs are never 100% optically efficient, but maximizing the transmittance results in more power at the output plane.

The POFs are produced by computing the MSF and then normalizing each point in the filter by the absolute magnitude at that point, $F_{POF}(p,q) = F^*(p,q)/|F(p,q)|$. The magnitude normalization produces a filter with unity magnitude at all points, which gives 100% optical efficiency.

The Binary Phase Only Filters (BPOF) are generated by examining the sign of the cosine of the phase of the MSF at each point and assigning a value of +1 or −1. The resulting filter pattern is both real and symmetric, and has no attenuation since it has unity magnitude at all points. The real and symmetric properties of the BPOF are similar to the properties of a cosine transform of the filter function.[19] The BPOF contains both the filter function spectrum and the complex conjugate of the filter function spectrum.

After the appropriate filter spectrum has been generated, a point–by–point complex multiplication is then performed on the FFT of the input scene and the complex conjugate of the filter spectrum. This simulates the spatial filtering operation which occurs at the frequency plane in an optical correlator. The filtered signal is then inverse FFT'd back to the space domain. The resulting image is the output electric field from the simulated correlator. The electric field is a complex quantity which cannot be directly measured, but the intensity of the image can be measured. The output image intensity is calculated by multiplying the output electric field by its complex conjugate.

Only a portion of the output image, which contains 128×128 elements, contains useful information. The input image and spatial filter pattern were zero padded to avoid wraparound error. The output plane only contains 64×64 elements of useful information. The appropriate choice of the input scene and filter pattern within the 128×128 arrays yields the output image within the first 64×64 elements of the output array, see figure 7. The MSF and POF filters are complex functions which are symmetric across the 128×128 array. The product of these functions with the input scene followed by the inverse FFT operation produces only a 64×64 subarea of useful information.

The situation is slightly different when BPOF's are used at the filter plane. The BPOF is a real and symmetric function which will give a symmetric result after being inverse FFT'd. The output plane of an optical correlator using a BPOF at the frequency plane will possess some symmetry. The symmetry manifests itself as an inverted copy of the filter pattern at the conjugate position of the filter pattern. The inverted copy produces the convolution of the input scene with an inverted copy of the filter pattern. This information is located in the region (65–128, 65–128) on the output plane, see figure 7. This subarea of the output plane is usually ignored in the computer simulation.

The output plane intensity distribution from the pc computer simulation is displayed in an isometric 3–D bar graph. The 3–D bar graph accurately represents the discrete nature of the data. The plotting routine is written in Fortran 77 using the Halo[44] graphics primitives library. These plots enable easy visual evaluation of the output intensity distribution. A sample output for a MSF in the optical correlator is given in figure 8. The graphs typically cover the range x:1–64, and y:1–64, which contains the desired output information.

The total energy output for the MSF is approximately half of the input plane energy. The optical efficiency of the MSF is not 100%, so some attenuation is expected. The POFs give 100% optical efficiency, therefore, the output plane energy is identical to the input plane energy. The BPOFs are also 100% efficient, however, the output plane information is spread over the two subareas (1–64, 1–64) and (65–128, 65–128). The total energy is conserved over the entire output plane, approximately equally divided between the two subareas.

The optical correlator simulation on the CRAY–XMP computer is very similar to the pc simulation. The flow chart for the simulation is given in figure 4b. The CRAY simulation uses 256×256 element arrays, which contain 128×128 points of useful information. The input scene data for the CRAY simulation is obtained by multiple calls to the subroutine used for generating the particle image record. After all the input particle images have been written to the input scene array, the input scene is Fourier transformed. The Fourier transformed input scene is stored in a complex array. The simulation now enters a loop where the filter pattern parameters are sequentially varied. The input scene data must be searched over a range of vector magnitudes and angles. There are three loops used to generate the filter patterns. The first loop selects the spacing S1. The second loop picks the spacing S2. The value of S2 ranges from S1/2 to S1/2 − 1. This accounts for any pixel rounding off errors in the digitized PIV transparency. The third loop selects the angle range on $\theta$. Due to the limited pixel resolution, the number of unique velocity vectors which must be searched varies with the magnitude of the velocity vector. For small interrogation vector magnitudes, the angle increment between unique vectors is large. A unique vector is defined as a vector which occupies at least one new pixel location compared to the previous vector. For a given velocity vector magnitude, the program increments the angle $\theta$ by 1°, and calculates the coordinates of the particle images in the filter pattern. If the new coordinates are not different from the old coordinates the angle is incremented again. This process is repeated until a unique particle image record is found.

The unique filter patterns covering the range of expected velocity magnitudes and angles are sequentially generated, Fourier transformed, point–wise multiplied by the Fourier transformed input scene array, and then the filtered signal is inverse Fourier transformed. This procedure of generating filter patterns and taking the product of the input scene spectrum and the filter spectrum simulates the sequential display of BPOFs on a light valve in an actual coherent optical processor. For each filter pattern generated, the output plane intensity distribution is calculated and scanned for correlation peaks. Each point in the output plane is compared to a threshold level. When a peak exceeds the threshold level, three quantities are stored in three independent arrays. The elements of the arrays correspond to each pixel on the output plane in the simulated correlator. The current filter angle and magnitude settings are stored in

two different arrays corresponding to the indices of the detected correlation peak. In addition, the correlation peak amplitude is stored at the detected peak position in another array. Before a detected peak's parameters are stored, the current peak amplitude is compared with the value stored in the peak amplitude array. If the new value exceeds the stored value, the new data are stored. If the stored peak value is greater than the detected peak value the stored values are preserved. This comparison procedure ensures that the most probable velocity vector at a particular location is stored, where the probability is indicated by the correlation peak amplitude.

After all the filter patterns have been used, the vector magnitude and angle storage arrays contain the detected 2–D velocity vector map of the input scene. The arrays are written to a file and downloaded to a pc computer for graphing.

## Expected Output Plane Information

An analysis of the matched filtering operation for a PIV optical correlator will indicate the expected output response and signal to noise ratio of the output. The finite energy in the input signal should limit the correlation peak amplitude. Also, the correlation length of the interrogation signal should be related to the energy in the sidelobes. The calculated results will be compared to the pc simulations. The pc simulation requires 5.5 seconds to compute a 128×128 real to complex single precision FFT. The complex to complex inverse FFT takes 11 seconds to compute. The entire pc simulation program take 23 seconds to perform the optical correlation operation.

## 3–Pulse Exposure Sequence

For the triple pulse exposure scheme, the particle image is recorded at three instances in time. The time intervals between pulses are chosen to make the spacings non–symmetric. Our choice is to make the time interval ratio 2:1. Assuming a noise free background on the input scene, the functional form of the 2–D, 3–pulse signal is:

$$s(x,y) = \delta(x-x_1, y-y_1) + \delta(x-x_2, y-y_2)$$
$$+ \delta(x-x_3, y-y_3) \qquad (11)$$

however, we will assume no y– dependence to reduce the bookkeeping:

$$s(x) = \delta(x-x_1) + \delta(x-x_2) + \delta(x-x_3) \qquad (12)$$

The Fourier transform of s(x) is:

$$S(p) = e^{-ipx_1} + e^{-ipx_2} + e^{-ipx_3}. \qquad (13)$$

## 3–Pulse MSF

The MSF for this case is just the complex conjugate of the input signal spectrum, $F^*(p) = S^*(p)$. The filtering operation for the 3–pulse MSF case is:

$$S(p)\cdot F^*(p) = e^0 \quad + e^{ip(x_2-x_1)} + e^{ip(x_3-x_1)}$$
$$+ e^{-ip(x_2-x_1)} + \vdots \quad e^0 \quad + e^{ip(x_3-x_2)}$$
$$+ e^{-ip(x_3-x_1)} + e^{-ip(x_3-x_2)} + e^0 \qquad (14)$$

The diagonal terms are the matched terms, which cancel to yield the dc portion of the filtered signal. This dc component will become the correlation peak on Fourier transformation to the output plane. The off–diagonal terms are the sidelobe information. The filtered signal can be rewritten as:

$$S(p)\cdot F^*(p) = 3 + 2\cos[p(x_3-x_1)] + 2\cos[p(x_3-x_2)]$$
$$+ 2\cos[p(x_2-x_1)] \qquad (15)$$

The output electric field is obtained by inverse Fourier transforming the filtered signal:

$$\mathcal{E}_0(x) = \frac{1}{2\pi}\int_{-\infty}^{\infty} S(p)\cdot F^*(p)\cdot e^{ipx}\, dp \qquad (16)$$

$$\mathcal{E}_0(x) = \frac{1}{2\pi}\int_{-\infty}^{\infty} \{3 + 2\cos[p(x_3-x_1)] + 2\cos[p(x_3-x_2)]$$
$$+ 2\cos[p(x_2-x_1)]\}\cdot e^{ipx}\, dp \qquad (17)$$

$$\mathcal{E}_0(x) = \frac{1}{2\pi}\{3\cdot\delta(x) + \delta(x\pm(x_3-x_1)) + \delta(x\pm(x_3-x_2))$$
$$+ \delta(x\pm(x_2-x_1))\} \qquad (18)$$

The intensity is given by:

$$I_0(x) = \frac{1}{4\pi^2}\{9\cdot\delta(x) + \delta(x\pm(x_3-x_1)) + \delta(x\pm(x_3-x_2))$$
$$+ \delta(x\pm(x_2-x_1))\} \qquad (19)$$

Using a definition of SNR as the ratio of the correlation peak power to the sidelobe power, we find SNR = 1.5. The output plane from the computer simulation of the 3–pulse MSF case is shown in figure 8. The calculated SNR is identical to the estimate obtained from the pc simulation. The computer simulation output plane total energy is 1.667. The MSF is approximately 50% efficient.

## 3–Pulse POF

The triple pulse POF case should yield a larger SNR than the MSF case. Again, let the input scene contain s(x) as defined in equation 12, and define the POF as:

$$F_{POF}(p) = \frac{S^*(p)}{|S(p)|} \qquad (20)$$

The filtering operation for the "matched" case is:

$$S(p) \cdot F_{POF}(p) = \frac{S(p) \cdot S^*(p)}{|S(p)|} = \frac{|S(p)|^2}{|S(p)|} = |S(p)|$$

(21)

$$= [S(p) \cdot S^*(p)]^{\frac{1}{2}}$$

The optical correlator output electric field is given by:

$$\mathcal{E}_o(x) = \frac{1}{2\pi} \int_{-\infty}^{\infty} [S(p) \cdot S^*(p)]^{\frac{1}{2}} \cdot e^{ipx} \, dp$$

(22)

From the 3–pulse MSF case we know the form of $S(p) \cdot S^*(p)$, which when inserted into equation 22 gives:

$$\mathcal{E}_o(x) = \frac{1}{2\pi} \int_{-\infty}^{\infty} \{3 + 2\cos[p(x_3 - x_1)] + 2\cos[p(x_3 - x_2)]$$

$$+ 2\cos[p(x_2 - x_1)]\}^{\frac{1}{2}} \cdot e^{ipx} \, dp$$

(23)

There is no known closed form solution for this integral. The kernel of the transform can be rewritten in the form $(1+x)^{\frac{1}{2}}$ and then approximated by

$$(1+x)^{\frac{1}{2}} \approx 1 + \frac{1}{2} \cdot x - \frac{1}{8} \cdot x^2 + \frac{1}{16} \cdot x^3 - \dots$$

(24)

Using the first two terms in the approximation we find:

$$\hat{\mathcal{E}}_o(x) = \frac{3^{\frac{1}{2}}}{2\pi} \int_{-\infty}^{\infty} \left\{ 1 + \frac{1}{6} \Big[ 2\cos[p(x_3 - x_1)] + 2\cos[p(x_3 - x_2)] \right.$$

$$\left. + 2\cos[p(x_2 - x_1)] \Big] \right\} e^{ipx} \, dp$$

(25)

where $\hat{}$ denotes an approximate representation of the actual function. A closed form solution for the Fourier transform in equation 25 exists and the result is:

$$\hat{\mathcal{E}}_o(x) = \frac{3^{\frac{1}{2}}}{2\pi} \cdot \left[ \delta(x) + \frac{1}{6} \cdot \delta(x \pm (x_3 - x_1)) + \frac{1}{6} \cdot \delta(x \pm (x_3 - x_2)) \right.$$

$$\left. + \frac{1}{6} \cdot \delta(x \pm (x_2 - x_1)) \right]$$

(26)

The intensity is:

$$\hat{I}_o(x) = \frac{3}{4\pi^2} \cdot \left[ \delta(x) + \frac{1}{36} \cdot \delta(x \pm (x_3 - x_1)) + \frac{1}{36} \cdot \delta(x \pm (x_3 - x_2)) \right.$$

$$\left. + \frac{1}{36} \cdot \delta(x \pm (x_2 - x_1)) \right]$$

(27)

The estimated SNR using this approximation is SNR = 6.0. The output from the computer simulation for this 3–pulse POF case, shown in figure 9, gives a SNR = 5.81. The approximation appears to be pretty close for this case. The information we are interested in is why the POF gives smaller sidelobes than the MSF. The signal in the POF case is of the form $(1+x)^{\frac{1}{2}}$. The square root operation reduces the sidelobe amplitudes relative to the correlation peak amplitude. The estimated value of

the SNR = 6.0 will approach the computer simulation value of 5.81 as more higher order terms are included in the approximation. The higher order terms produce more off–axis sidelobes on the output plane. The input scene total power is conserved in this 3–pulse POF simulation, since the total output energy is 3.0.

### 3–Pulse BPOF

A direct analytical study of the BPOF or HBPOF is not feasible. A 3–pulse BPOF computer simulation result is shown in figure 10. The distribution of sidelobes is not in a linear fashion as in the POF case. The sidelobes are distributed randomly around the correlation peak. The BPOF SNR is 2.35, which is approximately half the value obtained with the continuous POF. This is due to the symmetry of the BPOF. The BPOF spectrum contains both the interrogation pattern spectrum and the conjugate of the interrogation pattern spectrum. Hence, for the matched case ($F(p,q) = S(p,q)$), the input scene is cross correlated with the filter function $S(p) \cdot S^*(p)$ and also autocorrelated with itself $S^2(p)$. This means that half of the input scene energy is used in the autocorrelation and the other half is used in the cross correlation. This is the reason for the $\approx 50\%$ reduction in the SNR for the BPOF case over the POF case. The total output plane energy from the simulation in figure 10 is approximately 1.5. The total energy in the 64×64 array is only half of the input scene energy. Figure 11 shows the entire output plane of 128×128 points. The autocorrelation term at the conjugate position is readily observed. Also, the total energy is now accounted for. The BPOF is 100% optically efficient, but distributes the sidelobe energy in a different form than the continuous POF.

### 3–Pulse HBPOF

The HBPOF performance is very similar to that of the BPOF. The HBPOFs are phase only filters, so we expect 100% optical efficiency. The HBPOFs also contain the same conjugate symmetry as the BPOF. The HBPOF output will contain the desired filter spectrum plus the complex conjugate of the filter spectrum. The difference between the HBPOF and the BPOF is the sensitivity of the correlation peak amplitude to the filter pattern orientation angle $\theta$. The BPOF and HBPOF give identical results when $\theta = 0°$, or 90°, as in figure 10. However, as $\theta$ varies between 0° and 45° the BPOF correlation peak amplitude decreases, reaching a minimum at $\theta = 45°$, see figure 12. The energy loss in the correlation peak appears as an energy gain in the sidelobes, which reduces the SNR for the BPOF. Figure 13 shows the output plane light intensity distribution for the HBPOF under the identical conditions as figure 12. The HBPOF correlation peak value and SNR are essentially the same as for the $\theta = 0°$ case. At $\theta = 45°$, the BPOF correlation peak amplitude has decreased 6% over the value at $\theta = 0°$, while the HBPOF correlation peak amplitude increased by 0.8%. Both filters display equal performance at $\theta = 0°$, but as angle $\theta$ increases the BPOF degrades in performance. The HBPOF maintains its performance throughout the filter pattern angle orientation range. This feature is important for an optical correlator system which requires a minimum threshold level for signal detection. We want the correlation peaks to be as large as possible to give better noise discrimination. For the class of objects we are dealing with the HBPOF gives superior performance.

9

## 5–Pulse Patterns

The 5–pulse output plane intensity distributions are very similar to the 3–pulse cases discussed above. The main differences are an increase in both the correlation peak amplitude and the number of sidelobes. An anticipated benefit of the 5–pulse sequence is a reduction in the number of false correlations due to the random distribution of the recorded particle images. The requirement of 5 particle images being properly oriented is more stringent than for 3 particle images. The differences will be borne out in the CRAY simulation results.

## CRAY Simulation Results

The output data from the CRAY simulation program is a 2–D velocity vector map of the input particle image transparency. The input scene chosen for the simulation is a four quadrant swirling flow. The velocity vector map for this flow field is shown in figure 14. The four swirl pattern was generated using a solid body rotation in each quadrant. The velocity varies with radius. The vector positions were determined using a random number generator. The input scene contains 79 velocity vectors in a 128×128 array. The angle range encompasses a full 360°. The particle image separations (S1) range from 2 pixels to 12 pixels.

The input scene contains the images of the particles in the swirling flow at the instances in time that the light sheet is pulsed. The four swirl input scene for a 3–pulse exposure is shown in figure 15. This is the scene that the optical correlator must scan and identify the images corresponding to a unique particle. A few of the outliers are easy to identify. However, closer to the center of the swirls, the three images of the same particle are more difficult to identify.

The results obtained from the pc simulations were used to select the HBPOFs and to set the minimum threshold level for a detection. For the 3–pulse case the threshold level is 0.97. For the 5–pulse case the threshold level is 1.35. These are the minimum threshold levels. The detected correlation peaks may be larger than these minimum levels. The source of variation in the correlation peak amplitude is from the overlapping sidelobes from other partial correlations. Another source of correlation peak variation is the angular dependence of the correlation peak. This angular variation is minimized by using the HBPOFs.

From the required searching ranges on S1 (10 values), S2 (2 values for each S1), and $\theta$ (360 angles for each S1 and S2), the number of velocity vectors to be searched is 7200. The number of unique velocity vectors determined and searched by the simulation program is 1221. The total CPU runtime for both the 3– and 5–pulse simulations is 229 seconds. This corresponds to approximately 0.18 seconds per interrogation pattern.

The results from the 3–pulse 2:1 ratio spacing pattern are shown in figure 16. This 2–D velocity map contains many false and missed correlations. There are 48 correctly identified vectors, 32 missed vectors, and 69 falsely identified vectors. These results are unacceptable. The random location of the particle images results in many false correlations for the 3–pulse pattern.

The 2–D velocity vector map from the 5–pulse 2:2:1:1 case is shown in figure 17. There are 79 total vectors detected in this output map. There are 74 correctly identified vectors, 5 missed vectors, and 5 falsely identified vectors. These results are very good, 87% of the input data vectors have been correctly identified. The lower number of falsely identified vectors for the 5–pulse case is attributed to the lower probability of the random particle locations satisfying the required 5 particle image positions in the pattern.

Of the 74 correctly identified velocity vectors, there were no errors in determining the velocity magnitude. The HBPOFs are very sensitive to scale and rotation. The detected angles did not exactly agree with the input data. This is not a detection error, but is a quantization error. The limited resolution of the arrays used reduces the angular resolution. The program skips some angles because they do not produce unique velocity vector patterns. The variation between the detected angle and the actual angle occurs when the actual angle lies between two unique velocity vectors as determined by the computer. This is an inherent limitation due to the discrete nature of the process. Higher resolution arrays will decrease these quantization effects.

## Conclusions

The results of a computer simulation of optical correlation techniques applied to the reduction of particle imaging velocimetry transparencies has been presented. An asymmetric pulse exposure scheme allows the velocity vector direction to be unambiguously determined. The 5–pulse exposure sequence yielded a high quality 2–D velocity map with few false correlations. Hartley binary phase only filters were used to simulate the operation of a spatial light modulator placed at the frequency plane in the optical correlator. Although the simulations were intended to model the operation of an optical correlator employing a spatial light modulator, the digital evaluation of the transparencies is also a viable technique. For the digital evaluation, the input scene transparency can be digitized and supplied to the computer program. The required processing time varies directly with the range of velocity vector magnitudes and angles which must be searched. Future work will involve optically recording a 5–pulse exposure PIV transparency and processing the transparency using both the optical correlator employing a spatial light modulator, and a digital analysis on the computer.

## References

1) Leendertz, J. A.;"Interferometric displacement measurement on scattering surfaces utilizing speckle effect", J. Phys. E 3, p214, 1970.

2) Ineichen, B., Elgin, P., Dändliker, R.;"Hybrid optical and electronic image processing for strain measurements by speckle photography", Appl. Opt. 19, p2191, 1980.

3) Barker, D. B., Fourney, M. E.;"Measuring fluid velocities with speckle patterns", Optics Lttrs 1, pp 135–137, 1977.

4) Dudderar, T. D., Simpkins, P. G.;"Laser speckle photography in a fluid medium", Nature 270, pp 45–47, 1977.

5) Meynart, R.;"Equal velocity fringes in a Rayleigh–Bernard flow by a speckle method", Appl. Opt. 19, p1385, 1980.

6) Meynart, R.;"Speckle velocimetry study of vortex pairing in a low–Re unexcited jet", Phys. Fluids 26, p2074, 1983.

7) Meynart, R.;"Instantaneous velocity field measurements in unsteady gas flow by speckle velocimetry", Appl. Opt. 22, p535, 1983.

8) Adrian, R. J., Yao, C. S.;"Development of pulsed laser velocimetry (PLV) for measurements of fluid flow" *Eighth Biennial Symposium On Turbulence*, Sept. 26–28 1983, U. Missouri Rolla, J. L. Kakin and G. K. Patterson, Eds.

9) Adrian, R. J., Yao, C. S.;"Pulsed laser technique application to liquid and gaseous flows and the scattering power of seed materials", Appl. Opt. 24, p44, 1985.

10) Yao, C. S., Adrian, R. J.;"Orthogonal compression and 1–D analysis technique for measurement of 2–D displacements in pulsed laser velocimetry", Appl. Opt. 23, p1687, 1984.

11) Adrian, R. J.;"Image shifting technique to resolve directional ambiguity in double–pulsed velocimetry", Appl. Opt. 25, p3855, 1986.

12) Landreth, C. C., Adrian, R. J., Yao, C. S.;"Double pulsed particle image velocimeter with directional resolution for complex flows" *Tenth Biennial Symposium On Turbulence*, Sept. 22–24, 1986, U. Missouri Rolla.

13) Coupland, J. M., Pickering, C. J. D., Halliwell, N. A.;"Particle image velocimetry: theory of directional ambiguity removal using holographic image separation", Appl. Opt. 26, p1576, 1987.

14) Goodman, J. W.; *Introduction to Fourier Optics*, McGraw–Hill Book Pub., New York, 1968.

15) Oppenheim, A. V., Lim, J. S., Proc. IEEE 69, pg 529, 1981.

16) Horner, J. L., Gianino, P. D.;"Phase Only Matched Filtering", Appl. Opt, vol 23, pg 812–16, March 1984.

17) Gianino, P. D., Horner, J. L.;"Additional Properties of the Phase–Only Correlation Filter", Opt. Eng., vol 23, pg695–97, December 1984.

18) Horner, J. L., Leger, J. R.;"Pattern Recognition With Binary Phase–Only Filters", Appl. Opt., vol 24, pg609–11, March 1985.

19) Psaltis, D., Pack, E. G., Venkatesh, S. S.;"Optical Image Correlation With a Binary Spatial Light Modulator", Opt. Eng., vol 23, pg 698, 1984.

20) Cottrell, D. M., Lilly, R. A., Davis, J. A., Day, T.;"Optical Correlator Performance of Binary Phase–Only Filters Using Fourier and Hartley Transforms", Appl. Opt, vol 26, pg 3755, 1987.

21) Jost, S. R.;"A New Light–Modulated Liquid Crystal Light Valve"; *J. of Appl. Phys.*, vol 49, October, 1978.

22) Mallory, W. R.;"Dynamic Spatial Filter for Optical Signal Processing Using a Liquid Crystal Light Valve", *Intern. Soc. for optical Engineering*, A83–22794 08–60, Aug 25, 1981.

23) Michaelson, J. D., Sawchuk, A. A.;"Non–Linear Optical Processing Using Liquid Crystal Light Valves", *Soc. of Photo–Optical Instrum. Engineers*, A81–32464 14–35, 1980.

24) Mok, F, Diep, J., Liu, H. K., Psaltis, D.;"Real–Time Computer Generated Hologram by Means of Liquid Crystal Television Spatial Light Modulator", Opt. Lttrs, vol 11, Nov. 1986.

25) Liu, H. K., Davis, J. A., Lilly, R. A.;"Optical–Data–Processing Properties of a Liquid Crystal Television Spatial Light Modulator", Opt. Lttrs, vol 10, Dec. 1985.

26) Tai, A. M.;"Low–Cost LCD Spatial Light Modulator With High Optical Quality", Appl. Opt., vol 25, 1986.

27) Ross, W. E., Snapp, K. M., Anderson, R. H.;"Fundamental Characteristics of the Litton Iron Garnet Magneto–optic Spatial Light Modulator", *Proc. Soc. Photo–Engineers* 388 55–64, 1983.

28) Flannery, D., Keller, P., Cartwright, S., Loomis, J.;"Characterization of Improved Binary Phase–Only Filters in a Real–Time Coherent Optical Correlation", SPIE vol 753, *Acousto–Optic, Electro–Optic, and Magneto–Optic Devices and Applicat*, 1987.

29) Cottrell, D. M., Davis, J. A., Schamschula, M. P., Lilly, R. A.;"Multiplexing Capabilities of the Binary Phase–Only Filter", Appl. Opt., vol 26, pg 934, 1987.

30) Gregory, D. A.;"Real–Time Pattern Recognition Using a Modified Liquid Crystal Television in a Coherent Optical Correlator", Appl. Opt., vol 25, pg 467–6

31) Keller, P., Flannery, D., Cartwright, S., Loomis, J.;"Performance of Binary Phase–Only Correlation on Machine Vision Imagery", SPIE vol 728, *Optics, Illumination, and Image Sensing for Machine Vision*, 1986.

32) Davis, J. A., Day, T., Lilly, R. A., Liu, H. K.;"Multichannel Optical Correlator/Convolver Utilizing the Magnetooptic Spatial Light Modulator", Appl. Opt., vol 26, pg 2479–83, 1987.

33) Davis. J. A., Heissenberger, G. M., Lilly, R. A., Cottrell, D. M., Brownell, M. F.;"High Efficiency Optical Reconstruction off Binary Phase–Only FiltersHughes Liquid Crystal Light Valve", Appl. Opt., vol 26, pg 929–33, 1987.

34) Flannery, D. L., Biernacki, A. M., Loomis, J. S., Cartwright, S. L.;"Real–Time Coherent Correlator Using Binary Magnetooptic Spatial Light Modulators atand Fourier PLanes", Appl. Opt., vol 25, pg 466, 1986.

35) Cottrell, D. M, Davis. J. A., Schamschula, M. P., Lilly, R. A.;"Multiplexing Capabilities of the Binary Phase–Only Filter, Appl. Opt., vol 26, pg 934–37

36) Mills, S. A., Ross, W. E.;"Dynamic Magneto–optic Correlator: Real Time Operation", SPIE vol 753, *Acousto–Optic, Electro–Optic, and Magneto–Optic Devices and Applications*, pg 54–63, 1987.

37) Javidi, B., Kuo, C. J.;"Joint Transform Image Correlation Using a Binary Spatial Light Modulator at the Fourier PLane", Appl. Opt., vol 27, pg 663–65,

38) Duthie, J. G., Upatnieks, J.;"Compact Real–Time Coherent Optical Correlators", Opt. Eng., vol 23, pg 7–11, January/February, 1984.

39) Ross, W. E., Psaltis, D., Anderson, R. H.;"Two–Dimensional Magneto–Optic Spatial Light Modulator for Signal Processing", Opt. Eng., vol 22, July/August1983.

40) Wernet, M. P., Edwards, R. V.;"Real Time Optical Correlator Using a Magnetooptic Device Applied to Particle Imaging Velocimetry", Appl. Opt., vol 27, pg 813–15, 1988.

41) Vander Lugt, A.;"Signal Detection by Complex Spatial Filtering", IEEE *Trans. Inform. Theory*, vol IT–10, pp139–145, 1964.

42) Horner, J. L., Bartlet, H. O.;"Two–Bit Correlation", Appl. Opt., vol 24, pg 2889, 1985.

43) Gonzalez, R. C., Wintz, P.;*Digital Image Processing*, Addison–Wesley Publishing Co., 1977.

44) Halo Graphics Kernel and Device Drivers Functional Description Manual, Version 2.26a, Media Cybernetics, Inc, 1986.
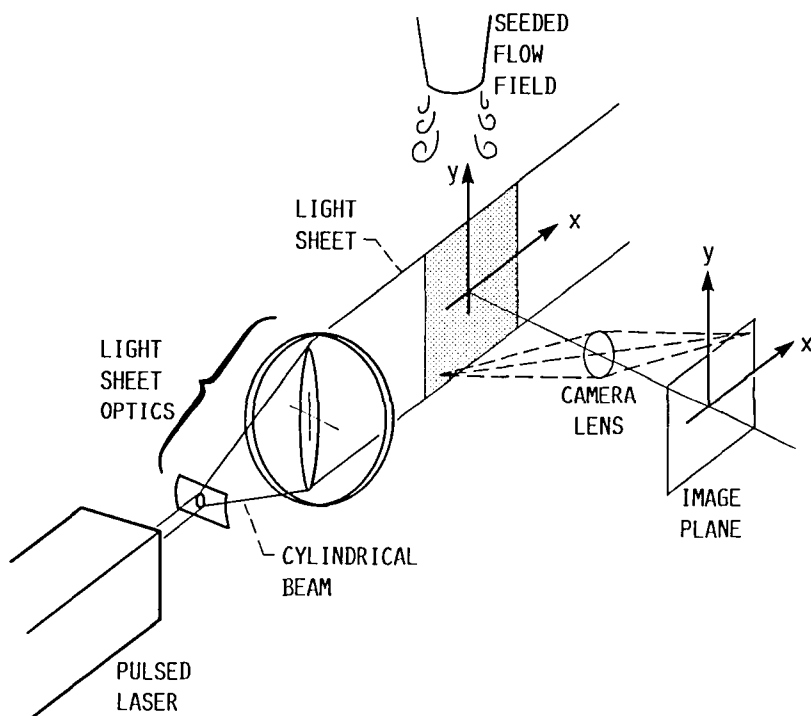
Figure 1:    Image recording system for a particle image velocimeter, or a laser speckle velocimeter.
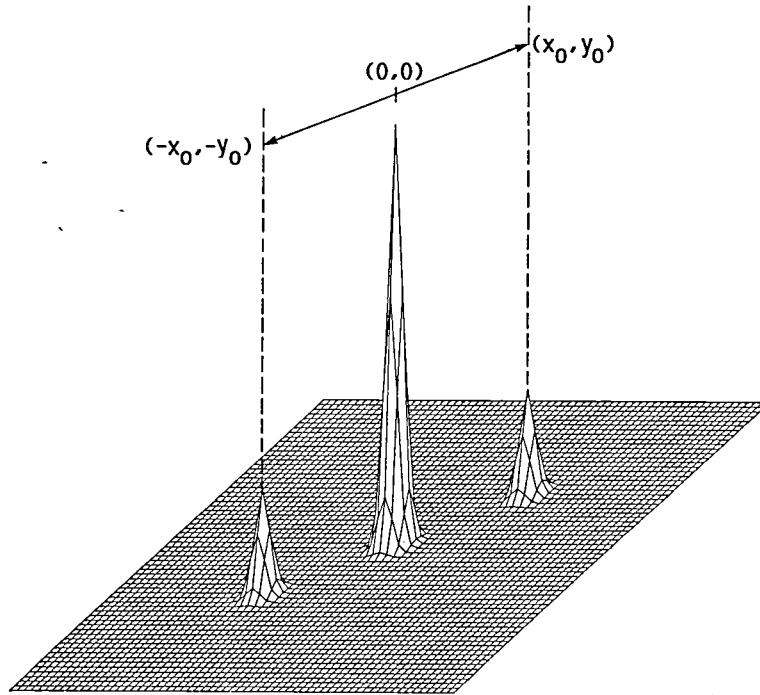
Figure 2: Light intensity distribution after Fourier transformation of a speckle fringe pattern. The power spectrum is symmetric. The average particle displacement is the distance $(x_0, y_0)$ along the line adjoining the central peak with the sidelobes. The velocity vector is indeterminate to $\pm 180°$.
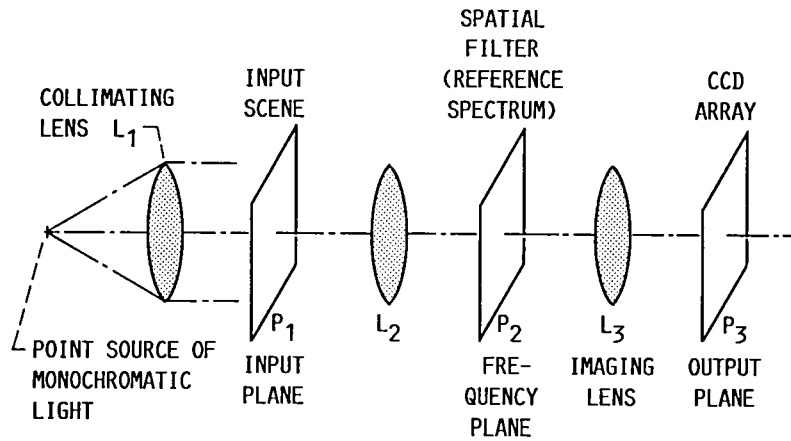


Figure 3: Optical arrangement of a coherent optical correlator. The PIV transparency is placed at the input plane ($P_1$). The spatial filter is placed at the frequency plane ($P_2$). The correlated output is observed on plane $P_3$.

13

**PC SIMULATION FLOW CHART**

Manual Input Scene
Data Entry: X,Y,S1,S2,θ

More
Data? — Yes

No

FFT and Store Input
Scene Spectrum

FFT Filter Pattern

Modify Filter Pattern

Point-Wise Multiply Filter
Spectrum With Input Scene
Spectrum

Inverse FFT
Filtered Signal

Calculate Intensity
Distribution

Generate Isometric
Bar Graph
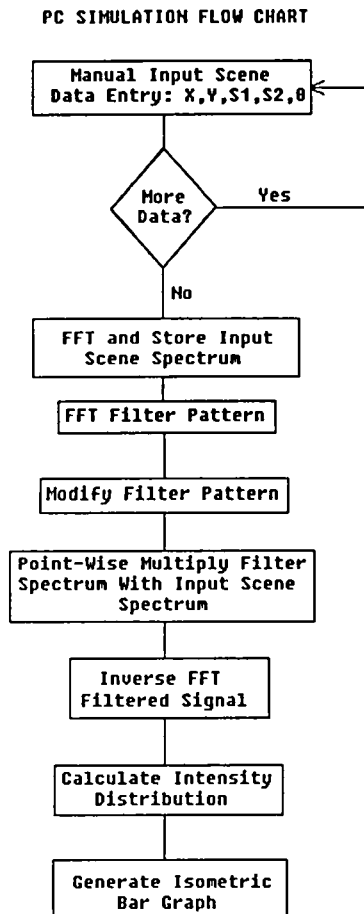
Figure 4a:     PC simulation flow chart.

**CRAY SIMULATION FLOW CHART**

Input Scene Array Data
Entry Via Subroutine
Calls

FFT and Store Input
Scene Spectrum

Begin Loop Execution
on Vector Magnitudes
And Angles

Is
New Vector
Unique? — No

Yes

FFT Filter Pattern

Modify Filter Pattern

Point-Wise Multiply Filter
Spectrum With Input Scene
Spectrum

Inverse FFT
Filtered Signal

Calculate Intensity
Distribution

Search Output Plane
For Correlation Peaks

Compare
Peaks To
Threshold
Level — Peak>Threshold? — Store Values
In Arrays At
Peak Location(s)

Peak<Threshold?

No

Finished
Searching
Through All
Possible
Vectors?

Yes

End Program

Figure 4b:     CRAY simulation flow chart.

14

TOTAL ENERGY = 3.0
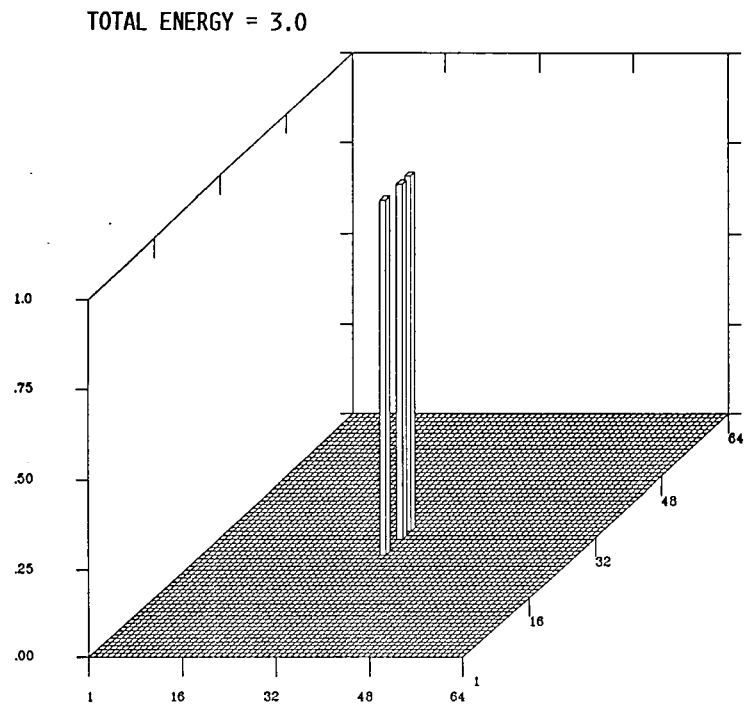
Figure 5:        3–pulse pattern (2:1 spacing ratio).
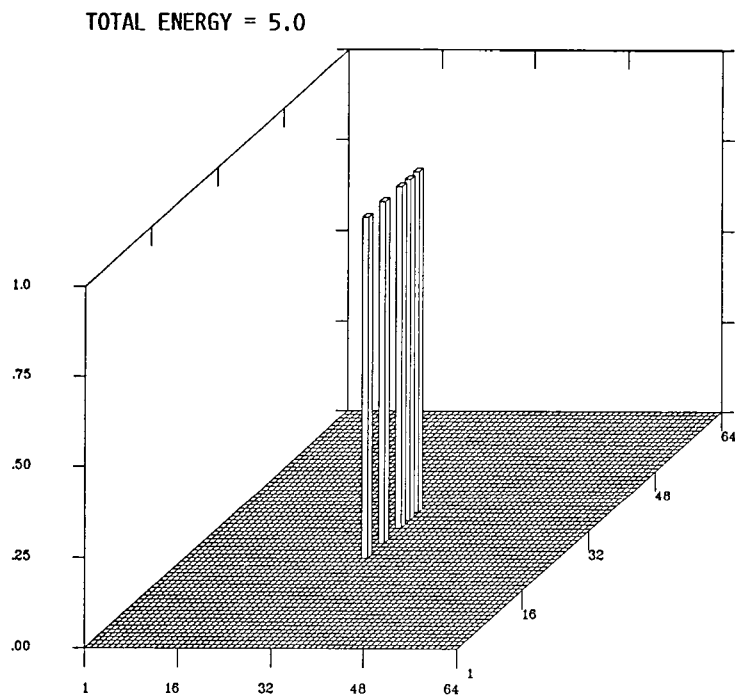
TOTAL ENERGY = 5.0

Figure 6:        5–pulse pattern (2:2:1:1 spacing ratio).

DATA PLACEMENT WITHIN THE SIMULATION ARRAYS
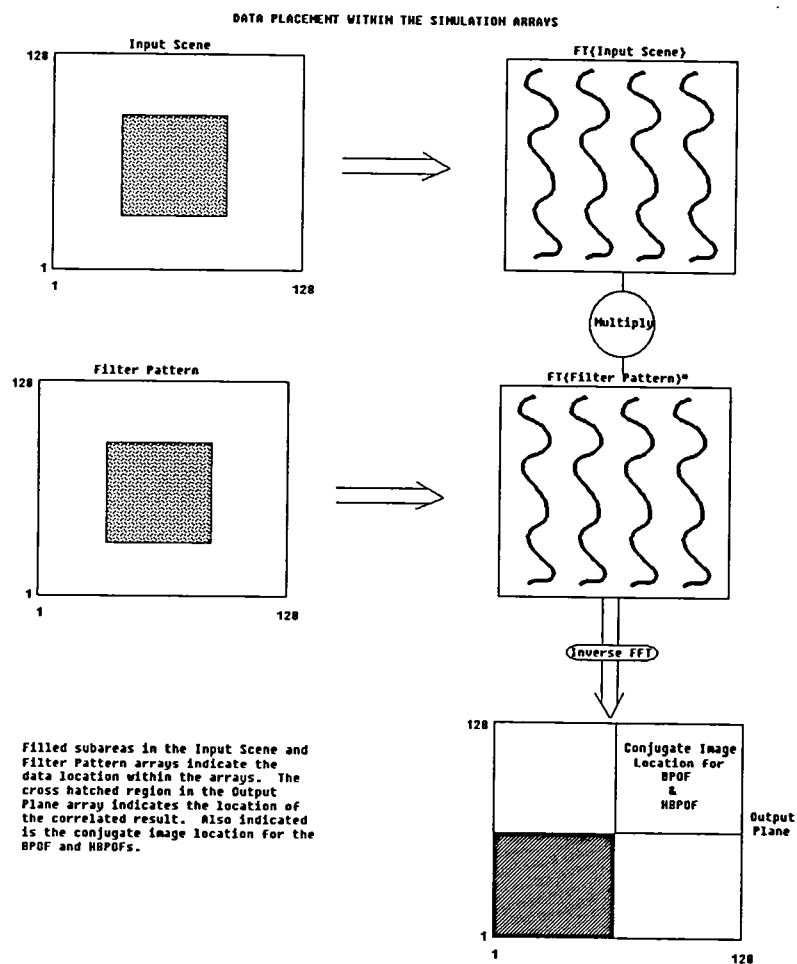


Figure 7: Relative placement of data within the 128×128 arrays used in the computer simulations.

PEAK AMPLITUDE = 1.000
SIDELOBE AMPLITUDE = 0.111
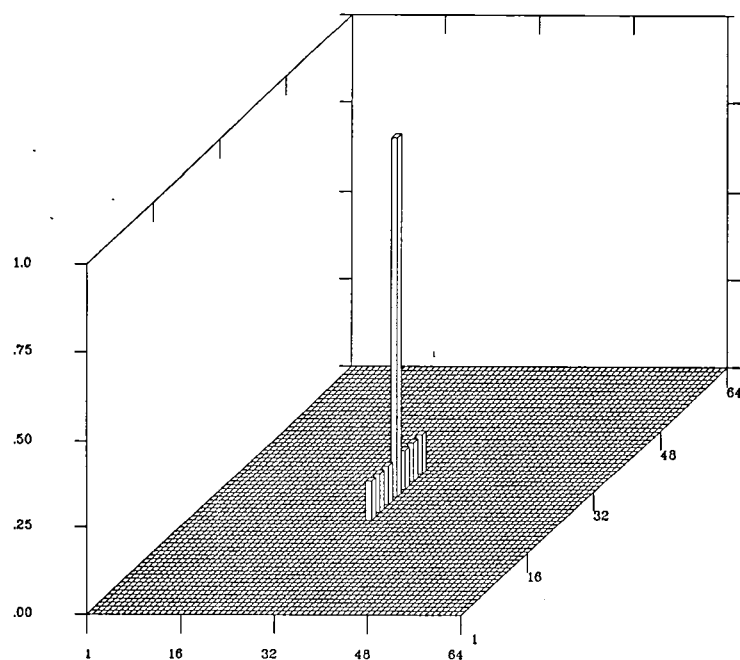SNR = 1.50
TOTAL ENERGY = 1.667

Figure 8: 3–pulse MSF output plane light intensity distribution for $\theta=0°$.

PEAK AMPLITUDE = 2.560
SIDELOBE AMPLITUDE = 8.59E-2
SNR = 5.81
TOTAL ENERGY = 3.000
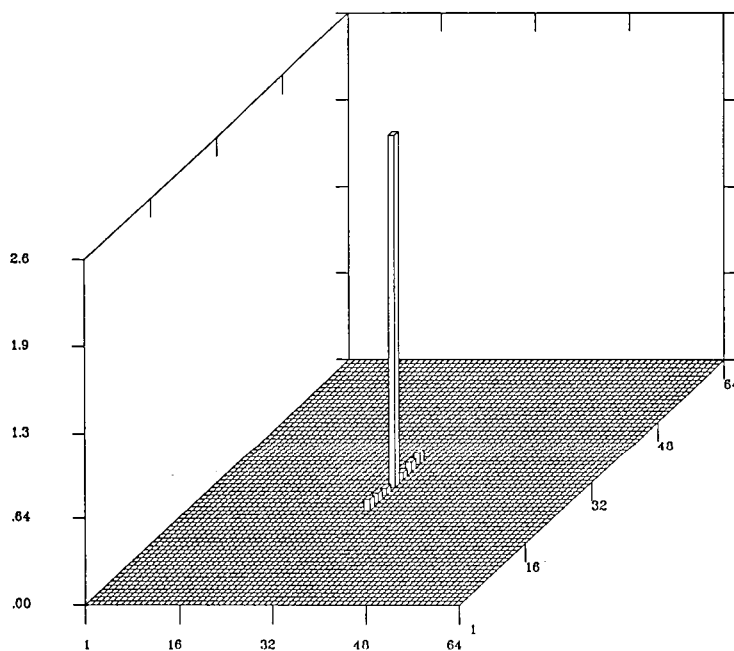
Figure 9: 3–pulse POF output plane light intensity distribution for $\theta=0°$. Note the lower sidelobes compared to the MSF case.

17

PEAK AMPLITUDE = 1.037
SIDELOBE AMPLITUDE = 5.109E-2
SNR = 2.35
TOTAL ENERGY = 1.479
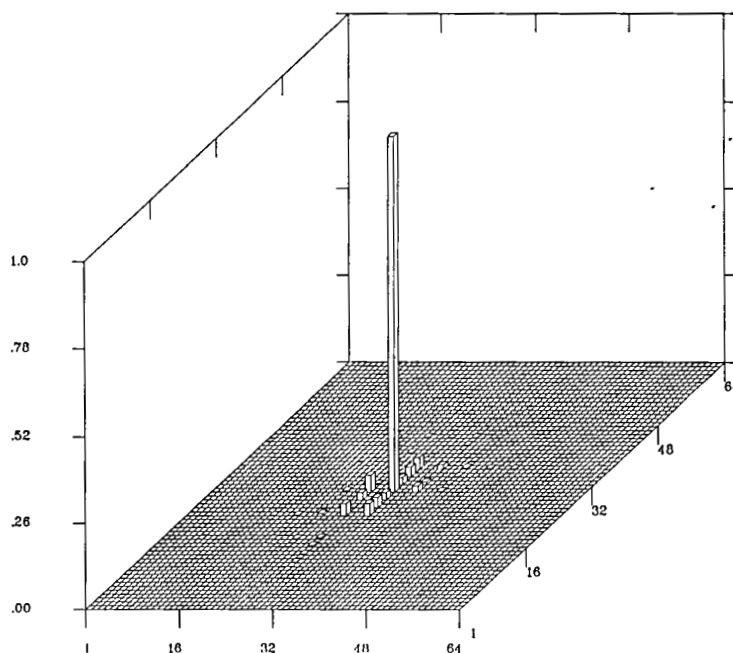
Figure 10:      3–pulse BPOF output plane light intensity distribution for $\theta=0°$. The sidelobes are randomly distributed about the correlation peak.

PEAK AMPLITUDE = 1.037
SIDELOBE AMPLITUDE = 5.109E-2
SNR = 0.53
TOTAL ENERGY = 3.000
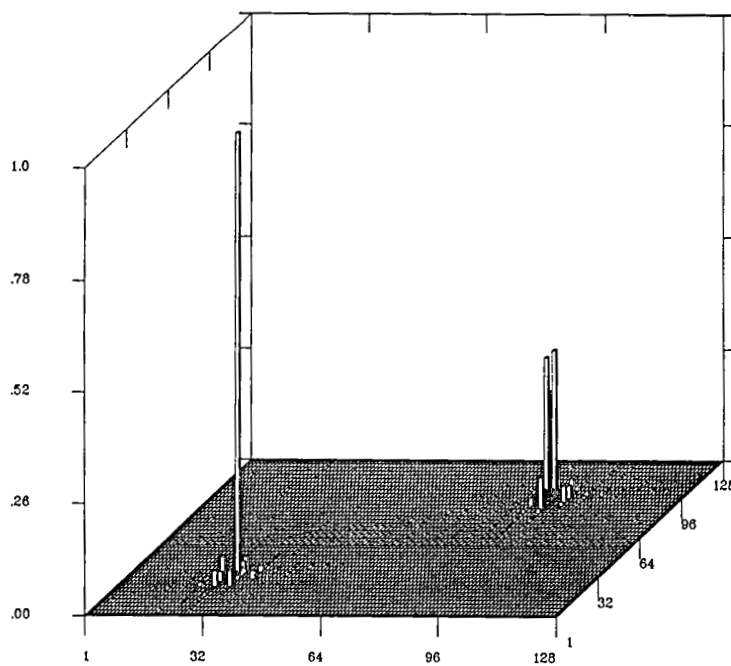
Figure 11:      3–pulse BPOF total (128×128) output plane light intensity distribution with conjugate image readily observable. The total input scene energy is conserved.

PEAK AMPLITUDE = 0.9758
SIDELOBE AMPLITUDE = 7.44E-2
SNR = 1.86
TOTAL ENERGY = 1.50
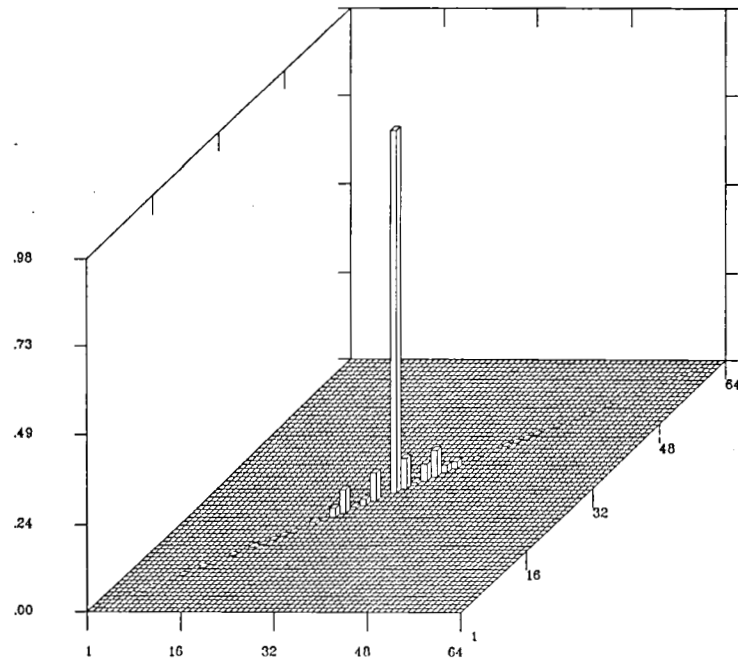
Figure 12:     3–pulse BPOF output plane for $\theta$=45°.

PEAK AMPLITUDE = 1.046
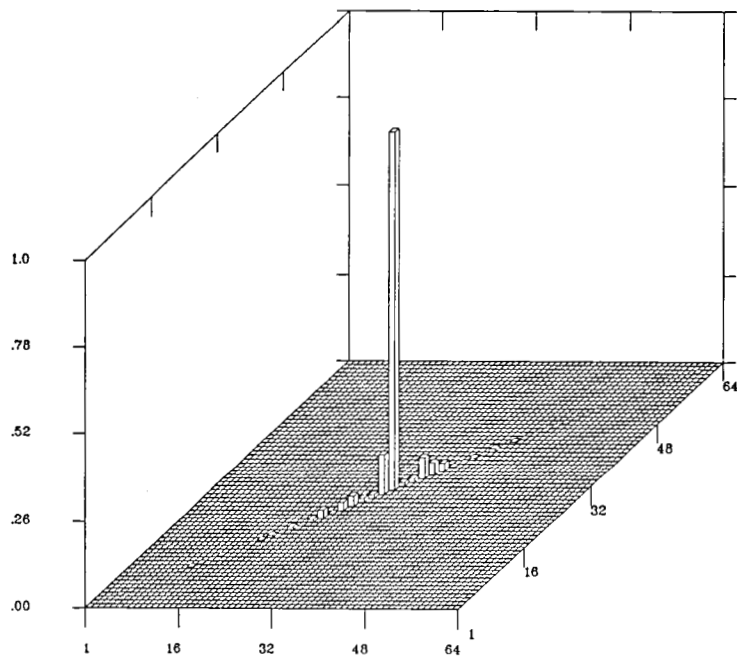SIDELOBE AMPLITUDE = 0.1163
SNR = 2.30
TOTAL ENERGY = 1.501

Figure 13:     3–pulse HBPOF output plane light intensity distribution for $\theta$=45°. Note the more rapid decay in sidelobe energy than for the BPOF case with $\theta$=45°. Also, the correlation peak amplitude is very close to the value for the BPOF case with $\theta$=0°.
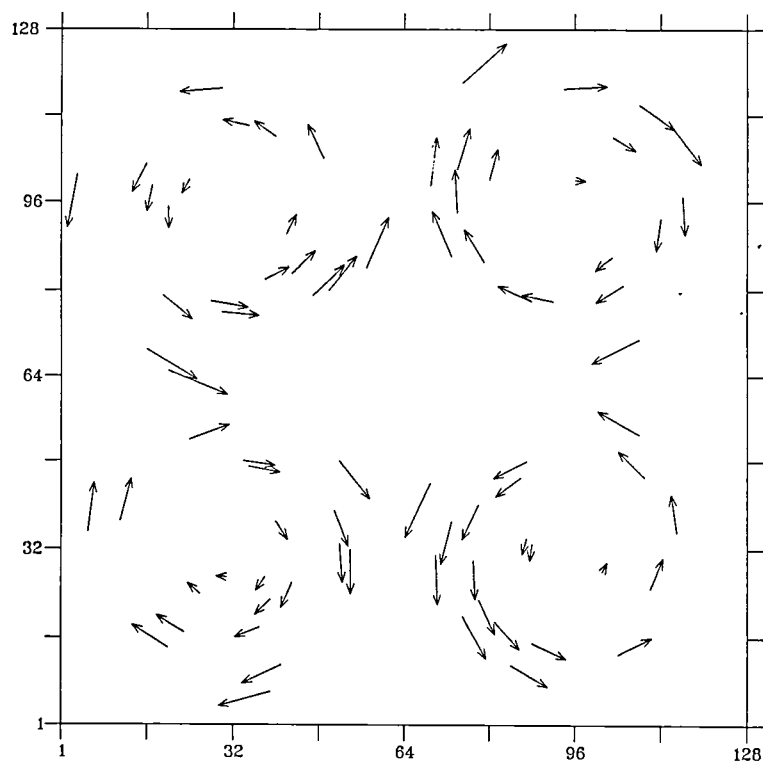
19

Figure 14:     2–D velocity vector map of input data to CRAY simulation.  There are 79 total vectors.
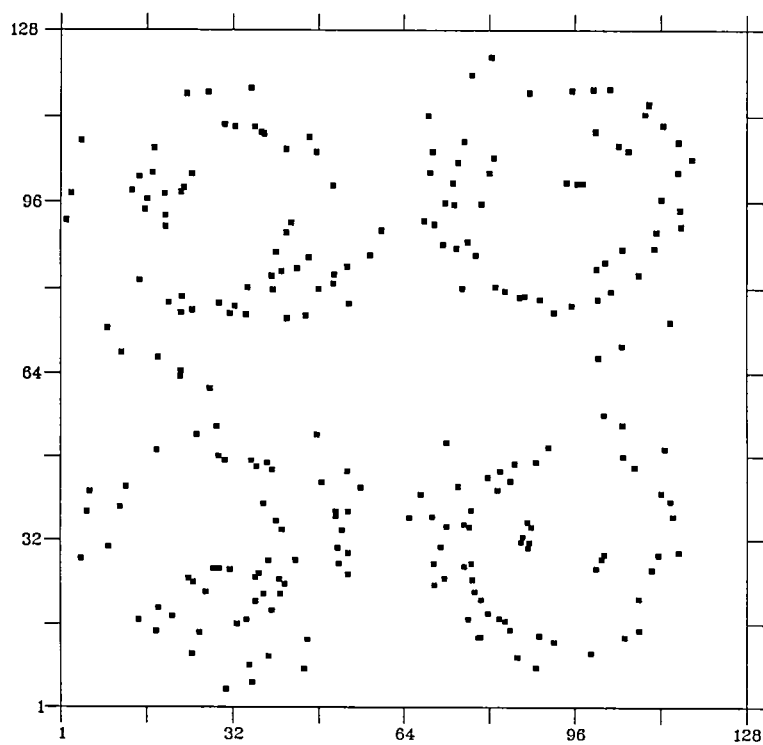


Figure 15:     Pixel plot of the input data to the CRAY simulation for the 3–pulse exposure case.  This plot represents the input scene transparency in the PIV optical correlator.
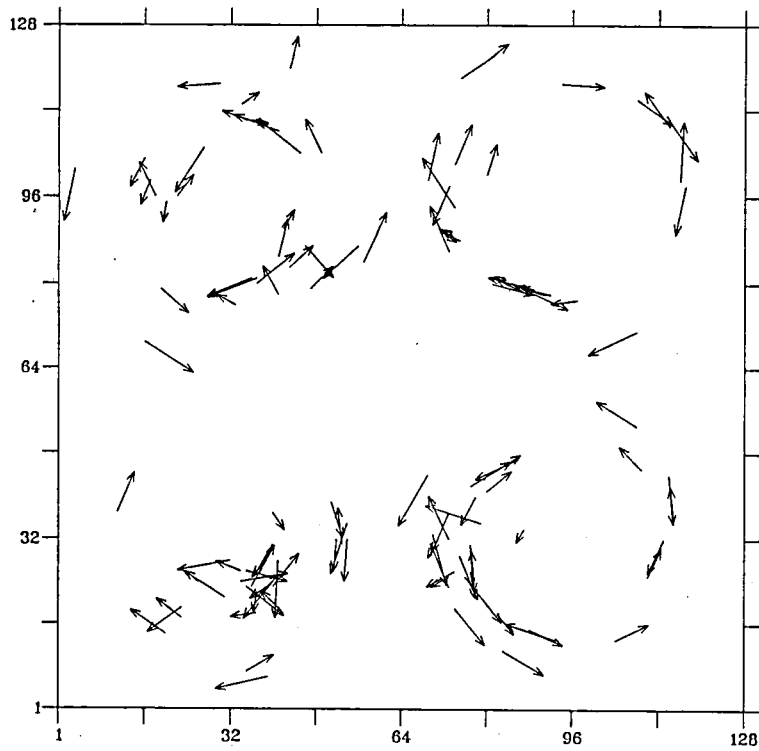
20

Figure 16:     Output velocity vector map for the 3–pulse HBPOF simulation. There are many false and missed correlations.
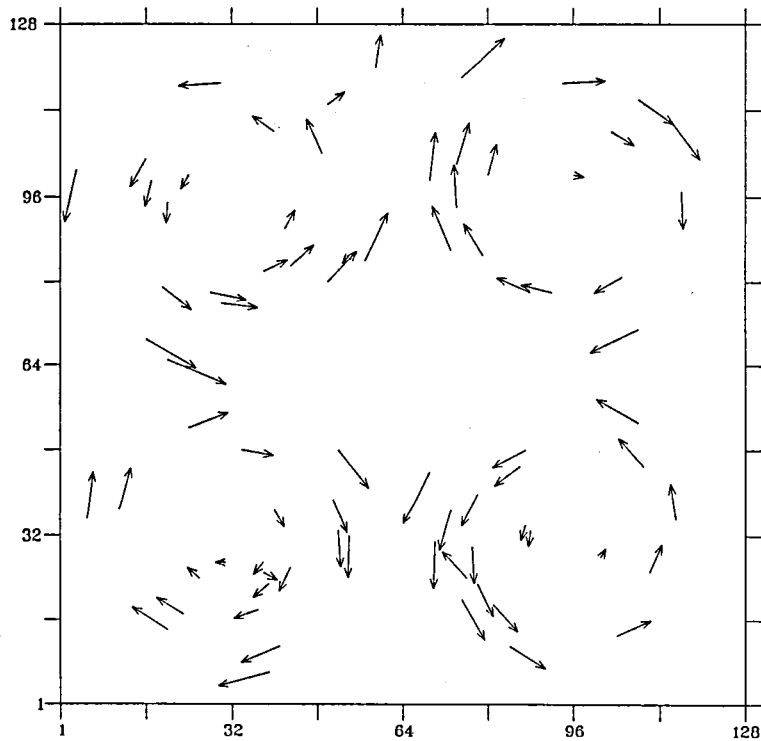


Figure 17:     Output velocity vector map for the 5–pulse HBPOF simulation. The 5–pulse exposure yields fewer false or missed correlations.

# NASA
National Aeronautics and
Space Administration

# Report Documentation Page

| 1. Report No. NASA TM-101306 | 2. Government Accession No. | 3. Recipient's Catalog No. |
|---|---|---|

| 4. Title and Subtitle | 5. Report Date |
|---|---|
| Application of Optical Correlation Techniques to Particle Imaging Velocimetry | 6. Performing Organization Code |

| 7. Author(s) | 8. Performing Organization Report No. |
|---|---|
| Mark P. Wernet and Robert V. Edwards | E-4297 |
| | 10. Work Unit No. 505-62-01 |

| 9. Performing Organization Name and Address | 11. Contract or Grant No. |
|---|---|
| National Aeronautics and Space Administration Lewis Research Center Cleveland, Ohio 44135-3191 | 13. Type of Report and Period Covered |

| 12. Sponsoring Agency Name and Address | Technical Memorandum |
|---|---|
| National Aeronautics and Space Administration Washington, D.C. 20546-0001 | 14. Sponsoring Agency Code |

15. Supplementary Notes

Prepared for the Conference on Sensors and Measurement Techniques for Aeronautical Applications cosponsored by the AIAA, NASA, and AFWAL, Atlanta, Georgia, September 7-9, 1988.

16. Abstract

Pulsed laser sheet velocimetry yields non-intrusive measurements of velocity vectors across an extended 2-dimensional region of the flow field. The application of optical correlation techniques to the analysis of multiple exposure laser light sheet photographs can reduce and/or simplify the data reduction time and hardware. Here, Matched Spatial Filters (MSF) are used in a pattern recognition system. Usually MSFs are used to recognize characters or assembly line parts. In our application, the MSFs are used to identify the iso-velocity vector contours in the flow. The patterns to be recognized are the recorded particle images in a pulsed laser light sheet photograph. Measurement of the direction of the particle image displacements between exposures yields the velocity vector. In this work, the particle image exposure sequence is designed such that the velocity vector direction is determined unambiguously. A global analysis technique is used in comparison to the more common particle tracking algorithms and Young's fringe analysis techniques.

| 17. Key Words (Suggested by Author(s)) | 18. Distribution Statement |
|---|---|
| Optical correlation Particle imaging velocimetry | Unclassified - Unlimited Subject Category 35 |

| 19. Security Classif. (of this report) | 20. Security Classif. (of this page) | 21. No of pages | 22. Price* |
|---|---|---|---|
| Unclassified | Unclassified | 22 | A02 |

National Aeronautics and
Space Administration

**Lewis Research Center**
Cleveland, Ohio 44135

**Official Business**
**Penalty for Private Use $300**

**FOURTH CLASS MAIL**

ADDRESS CORRECTION REQUESTED

LANGLEY RESEARCH CENTER

3 1176 01331 2443

NASA